CO_2 bubble generation and migration during magma-carbonate interaction

Blythe, L.S.[1,2], Deegan, F.M.[1,3], Freda, C.[4], Jolis, E.M.[1], Masotta, M.[5], Misiti, V.[4], Taddeucci, J.[4], Troll, V.R.[1,4]*

[1]Department of Earth Sciences, Centre for Experimental Mineralogy, Petrology, and Geochemistry (CEMPEG), Uppsala University, Uppsala, Sweden

[2]School of Physical and Geographical Science, Keele University, Keele, UK

[3]Department of Geological Sciences, Stockholm University, Stockholm, Sweden

[4]Istituto Nazionale di Geofisica e Vulcanologia (INGV), Rome, Italy

[5] Bayerisches Geoinstitut, Universität Bayreuth, Bayreuth, Germany

*Corresponding author. Email: valentin.troll@geo.uu.se; Telephone: +46 (0) 18 471 2570; Mail address: Department of Earth Sciences, Centre for Experimental Mineralogy, Petrology, and Geochemistry (CEMPEG), Uppsala University, Villavägen 16, 752 36, Uppsala, Sweden

1. Abstract

We conducted quantitative textural analysis of vesicles in high temperature and pressure carbonate assimilation experiments (1200°C, 0.5 GPa) to investigate CO_2 generation and subsequent bubble migration from carbonate into magma. We employed Mt. Merapi (Indonesia) and Mt. Vesuvius (Italy) compositions as magmatic starting materials and present three experimental series using i) a dry basaltic-andesite, ii) a hydrous basaltic-andesite (2 wt. % H_2O) and iii) a hydrous shoshonite (2 wt. % H_2O). The duration of the experiments was varied from 0 to 300 s and carbonate assimilation produced a CO_2-rich fluid and CaO-enriched melts in all cases. The rate of carbonate assimilation, however, changed as a function of melt viscosity, which affected the 2D vesicle number, vesicle volume, and vesicle size-distribution within each experiment. Relatively low viscosity melts (i.e. Vesuvius experiments) facilitated efficient removal of bubbles from the reaction site. This allowed carbonate assimilation to continue unhindered and large volumes of CO_2 to be liberated, a scenario thought to fuel sustained CO_2-driven eruptions at the surface. Conversely, at higher viscosity (i.e. Merapi experiments) bubble migration became progressively inhibited and bubble concentration at the reaction site caused localised volatile over-pressure that can eventually trigger short-lived explosive outbursts. Melt viscosity therefore exerts a fundamental control on carbonate assimilation rates and, by consequence, the style of CO_2-fuelled eruptions.

Keywords: CO_2, carbonate assimilation, melt viscosity, bubble size distribution, eruption style

2. Introduction

Earth's long-term volatile cycle reflects mass exchange between the deep Earth and the atmosphere, with volcanoes representing the major agents of volatile transfer. When magma migrates through crustal rocks *en route* from the mantle to the surface, it interacts thermally, chemically, and mechanically with the surrounding rocks. If these rocks are volatile-rich, such as limestone and dolostone which contain structurally-bound CO_2, magma-crust interaction can liberate crustal volatiles into the magmatic system, where they will eventually be released to the atmosphere via eruption or degassing.

While long-term magmatic degassing constantly delivers volatiles to the atmosphere, magma-crust interaction, in turn, may drive fluctuating peaks of "extra" CO_2 sourced from the crust. The latter process has been recognised in the recent volcanic gas record at Merapi volcano, Indonesia (e.g. Troll et al. 2012) and at Vesuvius volcano, Italy (Iacono-Marziano et al. 2009) and is thought to have played a major role in perturbations to the global carbon cycle in Earth's past (Ganino and Arndt 2009; Svensen et al. 2009; Johnston et al. 2011; Lee et al. 2013).

Indeed, it has been suggested that CO_2 emissions were several times greater than at present in, e.g., the Cretaceous, which, by consequence, had a warmer climate (Johnston et al. 2011; Lee et al. 2013). Excess CO_2 outgassing in the Cretaceous notably cannot be explained by pure decarbonation of subducted materials alone, especially as this process is thought to be rather inefficient based on thermodynamic models (Kerrick and Connolly 2001). Although less pronounced than in some earlier periods of Earth's history, an imbalance still exists between the amount of CO_2 released during subduction and the amount of CO_2 emitted at arc volcanoes at present (Dasgupta 2013). Carbonate-rich upper crustal lithologies beneath arcs have therefore been considered a missing piece in the carbon-cycle puzzle (cf. Johnston et al. 2011; Troll et al. 2012; Dasgupta 2013; Lee et al. 2013). In addition to the repercussions for the global carbon cycle on a geological time-

scale, magma-carbonate interaction can also contribute to driving short-lived explosive eruptions at hazardous volcanoes besides Vesuvius and Merapi, including sites such as Popocatépetl, Mexico and Yellowstone, USA (Goff et al. 2001; Werner and Brantley 2003; Schaaf et al. 2005; Chadwick et al. 2007; Iacono Marziano et al. 2009; Deegan et al. 2010; Dallai et al. 2011; Troll et al 2012, 2013; Borisova et al 2013). In this context, carbonate assimilation causes the host magma to become progressively more potassic and silica undersaturated, however, the simultaneously produced CO_2-rich fluid phase is less well understood (e.g. Watkinson and Wyllie 1969; Freda et al. 2008; Gaeta et al. 2009; Mollo et al. 2010). The dynamic aspects of CO_2 bubble nucleation, growth, and transport during carbonate assimilation and their combined effects on volcanic activity have still to be fully resolved.

To investigate the textural and chemical evolution of CO_2 bubbles during carbonate assimilation, time-constrained, high pressure-temperature experiments at conditions appropriate for mid to upper crustal magma reservoirs have been carried out. Starting materials from Merapi and Vesuvius volcanoes were doped with carbonate fragments and demonstrated both rapid production of CaO-enriched melts and CO_2 vesiculation in the vicinity of the added carbonate (Deegan et al. 2010, 2011; Jolis et al. 2013). In order to better comprehend the overall dynamics of the volcanic system during CO_2-fuelled eruptions and to further assess the role of magma-crust interaction in the subduction carbon cycle, it is imperative to quantify how CO_2-rich fluids are produced and mobilised in crustal systems (cf. Freda et al. 1997, 2011; Johnston et al. 2011; Troll et al. 2012; Dasgupta 2013; Jolis et al. 2013; Lee et al. 2013). We carried out analyses of vesicle diameter, vesicle number, vesicle volume, and vesicle size-distribution on previously characterised time-monitored carbonate assimilation experiments for Merapi and Vesuvius volcanoes (Deegan et al. 2010; Jolis et al. 2013) and compare these experimental sets

directly for the first time. We then present a quantitative assessment of the controls on vesicle generation and mobility during crustal carbonate assimilation.

3. Geological Background

Merapi and Vesuvius volcanoes are characterised by carbonate-hosted magmatic plumbing systems, wherein magma-carbonate interaction has been identified through isotopic studies of erupted minerals (e.g. feldspar, pyroxene, and olivine) and fumarolic CO_2 (e.g. Chadwick et al. 2007; Iacono Marziano et al. 2009; Dallai et al. 2011; Troll et al. 2012, 2013; Borisova et al. 2013). Notably, both volcanoes also have a history of explosive behaviour and are in proximity to major population centres, i.e., Yogyakarta in central Java (3.5 M inhabitants) and Naples in central Italy (> 4 M inhabitants), making Merapi and Vesuvius significant threats to modern society.

Merapi is situated on the Eurasian plate, beneath which the Indian ocean plate subducts at a rate of 6 to 7 cm/yr (Tregoning et al. 1994). In central Java, crustal thickness is ~ 25 km (Curray et al. 1977) and Merapi sits at the margin of the Kendeng basin, which contains ≥10 km of upper crustal sedimentary strata (van Bemmelen 1949; Smyth et al. 2005). Tertiary marine strata, carbonates, volcanics, and volcaniclastics, probably similar to those outcropping in the nearby Djiwo hills, underlie Merapi volcano (van Bemmelen 1949; Hamilton 1979; Chadwick et al. 2007). The Merapi plumbing system consists of a plexus of magma pockets dispersed throughout the crust (Chadwick et al. 2013; Troll et al. 2013; van der Zwan et al. 2013) and calc-silicate xenoliths are frequent amongst the eruptive products, providing direct petrological evidence for magma-carbonate interaction in the mid to upper parts of the Merapi supply system (Camus et al. 2000; Chadwick et al. 2007; Deegan et al. 2010; Troll et al. 2013, 2015). Fumarole chemistry indicates that carbonate assimilation is ongoing (Allard 1983; Troll et al. 2012), and what is more, post-

earthquake fumarole emissions from the summit crater sampled in 2006 demonstrate exacerbated assimilation, likely as a consequence of crustal basement rupture (Troll et al. 2012). Notably, the highly explosive 2010 Merapi eruption lacks abundant carbonate and skarn xenoliths, but shows strong geochemical evidence for intense carbonate digestion (Borisova et al. 2013). This "100-year" event was associated with an enormous CO_2 output during the eruption (Surono et al. 2012), thus implying very efficient carbonate assimilation on that occasion.

Vesuvius is located in the Campania Province, Italy, where carbonate rocks extend from ≥2 km to at least 8 km depth (Zollo et al. 1996; Bruno et al. 1998; Auger et al. 2001; Peccerillo 2005). The current magma plumbing system is distributed over small chambers throughout much of the crust, e.g., between 8 and 22 km (Auger et al. 2001, Civetta et al. 2004). Geophysical data place the top of a magma chamber, which is of considerable horizontal extent, at ~8 km depth, i.e., at the base of carbonate crustal strata (Auger et al. 2001). A shallower (ca. 2 to 4 km) magma chamber fed older Plinian eruptions (e.g. Pompeii, AD 79; Avellino, 3,500 BP), making shallow crustal magma-carbonate interaction a distinct possibility (Barberi et al. 1981; Civetta et al. 2004; Scaillet et al. 2008). Skarn xenoliths are a common feature in Vesuvius erupted products and provide independent petrological evidence for magma-carbonate interaction (Fulignati et al. 2000, 2004 a,b; Del Moro et al. 2001; Iacono Marziano et al. 2009; Dallai et al. 2011). The addition of volatiles sourced from carbonate must therefore play a significant role in magma chamber dynamics, especially since the current magma residence depth is assumed to be 3 to 4 km, e.g., for the 1944 eruption (cf. Fulignati et al. 2004b; Scaillet et al. 2008). In line with this inference, present day fumarole emissions appear to record a considerable carbonate-derived CO_2 component (Iacono Marziano et al. 2009).

4. Methodology

4.1 Experimental methods and analytical techniques

Piston cylinder experiments were previously carried out at the High Pressure-High Temperature Laboratory of Experimental Volcanology and Geophysics at the Istituto Nazionale di Geofisica e Vulcanologia (INGV) in Rome, Italy (Deegan et al. 2010; Jolis et al. 2013). The experiments consisted of a carbonate fragment (ca. 6 to 10 mg) enclosed in pre-fused, powdered magmatic starting material (ca. 24 to 42 mg) that were placed together in a platinum capsule. In all charges, the carbonate clast and magmatic material were ~ 20 % and 80 % of the total volume in the capsule, respectively (Table 1). Analyses of all starting materials are reported in Table 2. The experiments were subsequently pressurised at room temperature to 0.5 GPa and then heated in two stages, from ambient temperature to 1180°C at a rate of 200°C/min, and at 20°C/min until the experimental temperature was reached. Three experimental series are compared here: i) a dry Merapi basaltic-andesite, ii) a hydrous Merapi basaltic-andesite (2 wt. % H_2O), and iii) a hydrous Vesuvius shoshonite (2 wt. % H_2O). Note that a total of 2 wt. % H_2O was added to the hydrous experiments to account for the likely range of hydrous subduction zone compositions. The starting materials were then allowed to react at the target conditions for 0, 60, 90, and 300 s. The experiments were terminated by shutting down the power source, which caused quenching at a rate of ~2000°C/min and allowed the textural interplay between limestone and melt to be preserved. For a full account of starting materials, experiment preparation, experimental procedure, and rationale, see Deegan et al. (2010, 2011) and Jolis et al. (2013).

After the experiments were terminated, the capsules were mounted in epoxy resin, abraded to remove the capsule, and then polished to expose the surface of the experimental products at approximately mid-capsule depth. Back-scattered electron images of the polished surface were acquired using a JEOL JSM-6500F Field Emission Gun Scanning

Electron Microscope (FEG-SEM) at INGV, Rome. As vesicle size varied over three orders of magnitude, image magnification was varied accordingly.

4.2 Image analysis and data treatment

The aim of this paper has been to generate quantitative textural data to complement previous studies that employ quantification of the vesicle characteristics of volcanic rocks (e.g. Gardner et al. 1999; Shea et al. 2010; Heap et al. 2014). Low magnification FEG-SEM images (as low as 15x magnification), covering the whole area of the exposed experimental charges, were used to measure the size of the largest vesicles. Conversely, images of increasingly higher magnification (up to 1500x) were used to measure smaller vesicles over progressively smaller areas. The number of images and the magnifications employed were modified for each sample to best capture its vesicle size distribution. First, a visual inspection of the entire experiment at variable magnifications ensured the absence of clusters of small bubbles. This step was followed by taking the highest magnification images from randomly selected portions of the experiments. We then measured the area of each high magnification image, including the areas of all chemical domains that contained vesicles, but excluded any area with remaining carbonate or calcite crystals. The area of all individual vesicles present in each high magnification image was also measured separately using the ImageJ software (Abramoff et al. 2004). Vesicles attached to the edge of the capsule were included in the count, whereas those on the edge of an image were excluded. The Heywood diameter (equivalent diameter of a non-circular object) or Feret diameter (largest diameter obtainable from the area of a near-circular object) was calculated for each vesicle. Since these two measurements are equivalent for near-spherical vesicles, we will refer to the Heywood diameter only from here. These diameter values were ordered with the largest first, and were assigned a cumulative number (C_n). To compensate for the smaller vesicle areas measured at high magnification, we corrected the number of bubbles

to represent the whole capsule using a correction factor (F_{corr}). In this process, bubbles with a large area in the lower magnification groups were removed from all successively higher magnification groups to prevent smaller bubbles being extrapolated over areas that were occupied by larger bubbles. This correction factor (F_{corr}) and the cumulative correction (C_{corr}) were then calculated for each magnification class as follows:

$$F_{corr} = Area_{capsule} / \Sigma\ Area_{image} \quad (1)$$

$$C_{corr} = C_n \,.\, F_{corr} \quad (2)$$

The cumulative correction value (C_{corr}) represents the theoretical number of bubbles present in the whole sample that are larger than any specific diameter (Figure 1) and accounts for any over- or under-estimation of bubble numbers produced in the measurement procedure. We used a Heywood diameter *vs*. cumulative correction plot for each magnification group to identify where bubble measurements from each subsequently higher magnification set appear. Since bubbles of almost all sizes were measured at least at two or three different magnifications, overlap between the magnification groups ensured the effectiveness of the area correction (Figure 1). Finally, one single curve was created for each experimental charge from all magnification groups by using (i) representative magnifications to define the different sections of the curve and (ii) favouring higher magnification curves for smaller vesicle domains. Unfortunately, during polishing of the experimental charge 445-V7 (Vesuvius, 300 s), part of the sample was lost and the data are thus incomplete for this run. To compensate for this shortcoming, the missing area was not included in higher magnification area measurements, but was included in the whole sample area measurement. For extrapolation of vesicles over the whole sample area, we assumed that the lost area simply had the same vesicle arrangement as that observed in the remaining sample.

This method of vesicle size and number estimation employs a 2D surface and assumes that the largest diameter of each vesicle was intersected to derive an “ideal” diameter that

forms the basis of our vesicle volume calculations. Our approach would introduce error into a 3D volume calculation as the largest diameter of each vesicle is not always intersected. Furthermore, as larger vesicles dominate the samples, the potential for smaller vesicles to be underrepresented in 3D is increased (e.g., Sahagian and Proussevitch 1998). The method employed here, however, produces an internally consistent data set for the experiments that is applicable for our purpose, but does not lend itself to accurate volume determinations.

5. Results

5.1 Textural observations

Here we provide a summary of the textural features recorded in the respective Merapi and Vesuvius experiments. This direct comparison of the two experimental studies is intended to consolidate the available information in Deegan et al. (2010, 2011) and Jolis et al. (2013).

All three experimental series record chemical interaction between carbonate and melt as a result of partial or total assimilation of the carbonate (Figure 2). Three compositional glass domains are identified: i) a Ca-normal glass, compositionally similar to the starting material, ii) a Ca-rich glass, which arises due to breakdown of carbonate in the melt, and iii) a contamination front of varying extent that usually marks the transition between the Ca-normal and Ca-rich domains (see Deegan et al. 2010 and Jolis et al. 2013 for full details). Assimilation of carbonate in these experiments is always accompanied by rapid vesiculation and the size and spatial distribution of the vesicles are related to the stage of the reaction. Notably, in the dry series experiments, the Ca-normal domain contains crystal-rich regions, which affects melt viscosity (see discussion also).

Merapi Dry Series

In the Merapi dry series, the degree of carbonate assimilation increases with increasing run time (i.e. from 0 s to 90 s), with the most extensive carbonate incorporation into the melt at 300 s (Figure 2 a-d). At 0 to 90 s, the remaining carbonate is usually highly fractured and rounded and can show spallation of small fragments into the surrounding Ca-rich glass. The contamination front is well defined in all experiments of this series. Vesicles are primarily located in the Ca-rich glass with small vesicles frequently found near the carbonate while larger vesicles occupy generally more distant regions in the capsules (e.g. Figure 3 a) and sometimes appear to concentrate at the contamination front. In fact, the contamination front frequently follows the profile of large bubbles (e.g. in the 60 and 300 s experiments; Figure 2 b, d), indicating that bubble growth and migration progressively drives the compositional interface away from the carbonate clast. Notably, a sub-set of smaller vesicles is also located in the crystal-rich domain (Figure 2 d).

Merapi Wet Series

In the Merapi wet series, the carbonate was no longer observed in the capsule by 90 s. The edges of the remaining carbonate in the 0 and 60 s runs are irregular, rounded, and also show spallation of carbonate clasts from the main carbonate fragment. Calcite crystals are present surrounding the remnant carbonate fragments in the 0 and 60 s experiments and display a dendritic texture, which probably relates to rapid quenching of the experiments (Figure 4 a).

The extent of the Ca-rich glass generally increases at the expense of the Ca-normal one with increasing run time (Figure 2 e-h). Ca-normal glass is observed enclosing areas of Ca-rich glass in the advanced time series, implying mingling of the two melts. The contamination front becomes wider and less defined at increasing experimental duration (cf. Deegan et al. 2010). Larger vesicles are located in both the Ca-rich and Ca-normal

glasses, with an overall preference for the capsule margins. Smaller bubbles also occur in both glass types. However, in the Ca-normal glass, the smaller bubbles are arranged at a distance from the contamination front in semi-parallel bands, but maintain the shape of the contamination front (Figure 4 b). In addition, as in the Merapi dry experiments, the contamination front frequently follows the profile of large bubbles (e.g. 60 s experiment; Figure 2 f), highlighting the effect of vesicle growth and migration on the distribution of Ca-enriched (contaminated) melt domains.

Vesuvius Wet Series

In the Vesuvius wet series, the carbonate fragment was completely digested at 0 s. Although part of the 300 s experiment disintegrated during sample preparation, but because no carbonate was present at 0, 60 and 90 s, we assume that the carbonate was also fully dissolved in the 300 s run. In comparison with the Merapi series, the Ca-rich and Ca-normal glasses are no longer defined and the contamination front is generally more diffuse, increasing in width as the experimental duration progresses (Jolis et al. 2013). Notably, the majority of vesicles at 0s, 60 s and 90 s are now in the Ca-normal glass. At 0 s there are some larger bubbles located in the Ca-rich glass, though the majority of smaller vesicles appear to be in the Ca-normal glass (Figure 5 a). At 300 s, Ca-rich glass is dominant in the experimental charge (see Jolis et al. 2013) and almost all vesicles are located there. Calcite crystals are present in the 0, 60, and 90 s experiments and show a dendritic texture due to quenching (Figure 5 b).

5.2 Bubble nucleation and growth

Vesicle diameter and the cumulative vesicle number (C_{CORR}) were obtained for each of the experimental series. In the Merapi dry series (Figure 6 a), the 300 s experiment contains the largest amount of small bubbles (< 5 μm) and overall, the size of the smallest

bubbles decreases with increasing experimental duration (from 2.5 μm at 0 s to 0.2 μm at 300 s). Conversely, the size of the largest bubbles increases with increasing experiment duration (from 330 μm at 0 s to 880 μm at 300 s) and only the 90 s experiment does not follow these trends.

In the Merapi wet series (Figure 6 b), the 300 s experiment contains the largest amount of bubbles less than 5 μm in size. The diameter of the smallest and largest bubbles increases from 0.1 μm at 60 s run to 0.4 μm at 300 s and from ~ 135 μm at 0 s to >1000 μm at 300 s, respectively. Both Merapi series show the total number of bubbles to increase with time, i.e., the 300 s experiments contain significantly more bubbles than the 0 s ones.

The Vesuvius wet series shows an analogous increase in maximum bubble size with time, but also a decreasing number of bubbles with increasing run time (Figure 6 c). The smallest bubble size in the Vesuvius wet series ranges from 0.1 μm at 0 s to 0.3 μm at 300 s, whereas the largest bubble size at 60 s is ~ 470 μm and ~ 610 μm at 300 s. The variation of the largest bubble size for the Vesuvius series (Figure 6 c) is therefore much less than in the two Merapi series (Figure 6 a, b). In this respect, vesicle diameter versus cumulative vesicle volume shows a general trend towards larger cumulative volumes associated with longer experimental duration for both of the Merapi series, as expected from the increasing degree of carbonate assimilation (Figure 7 a, b). In contrast, complete assimilation of carbonate is confirmed in the Vesuvius wet experiments by approximately equal cumulative bubble volumes in all experiments (Figure 7 c) and is consistent with the textural similarities to those Merapi experiments where extensive carbonate assimilation occurred (e.g. the 300 s Merapi experiments).

6. Discussion

6.1 Water and carbon dioxide solubility in Merapi and Vesuvius magmas

Given the presence of water and the addition of CO_2 to the experiments, it is important to consider volatile solubility in the starting materials to understand volatile exsolution and migration in the corresponding experiments (e.g. Dixon 1997; Vetere et al. 2011). For the Vesuvius wet series, the shoshonite melt can dissolve up to 7.9 wt. % H_2O at 1250 ºC and 0.4 GPa (Vetere et al. 2011). In the case of Merapi, a basalt can contain 8.5 wt. % H_2O at 1200 °C and 0.5 GPa (Newman and Lowenstern 2002) and an andesite up to 10 wt. % H_2O at 1200 °C and 0.5 GPa (Botcharnikov et al. 2006). With respect to these data, all experimental glasses are H_2O under-saturated (H_2O ca. 2 wt. %). However, the presence of CO_2, whose quantity increases with progressive carbonate assimilation, will reduce water solubility in the melts (e.g. Holloway and Blank 1994; Botcharnikov et al. 2005; Deegan et al. 2010; Jolis et al. 2013). Using the volatile solubility model of Papale et al. (2006), we calculated H_2O-CO_2 solubilities for the Merapi wet experimental series. For the given temperature and pressure conditions (1200 °C and 0.5 GPa) the Merapi wet experiments show a water solubility limit at 2.12 wt. % and a CO_2 solubility of 0.36 wt. %. As determined by Jolis et al. (2013), the Vesuvius wet experiments can dissolve up to 1.9 wt. % H_2O and 0.34 wt. % CO_2. The water solubility for the Merapi wet and Vesuvius experiments in the presence of CO_2 is thus very close to the initial ~ 2 wt. % H_2O of the hydrous starting material, implying that when volatile saturation is reached the evolving vapour phase is dominated by CO_2. This can also be shown by employing the method of Deegan et al. (2010) and Jolis et al. (2013) to calculate the maximum amount of CO_2 produced from carbonate breakdown in the experiments. Taking the average masses of the magmatic starting material and the carbonate used in each experimental series, we calculate that 4.29 mg CO_2 (7.02 wt.%), 4.28 mg CO_2 (7.0 wt.%), and 2.9 mg CO_2 (4.75 wt.%) can be produced for the Merapi dry, Merapi wet, and Vesuvius wet experiments, respectively. Carbon dioxide is thus more abundant in the experiments than H_2O (maximum 2 wt. %) and represents the critical vapour phase in all series presented here.

6.2 Carbonate dissolution and the influence of melt viscosity

The rate of $CaCO_3$ breakdown in magma is controlled by the removal of CO_2 from the reaction site. Studies of natural systems such as the Hortavær Igneous Complex (Norway) and Etna (Italy) have suggested that prolonged magma-carbonate interaction is permitted only if CO_2 is efficiently and continually removed from the reaction site (Barnes et al. 2003; 2005; 2009; Mollo et al. 2012; Heap et al. 2013). This is because decarbonation in a closed system would eventually slow down due to an excess of the reaction product. Although the removal of CO_2 in the experiments would eventually be constrained by the capsule, those experiments where the Ca-rich glass reaches the edge of the capsule show that bubbles were still found to grow larger with increased experiment duration, which suggests that outgassing is not yet limited by the capsules (cf. Figure 2).

In contrast, the experiments show that under the investigated conditions, carbonate dissolution began before the experimental target temperature was reached and thereafter progressed with increasing experimental run-time. We note that the break-down of carbonate is accelerated in the experiments over that of pure decarbonation because of reaction with magma. Bubble nucleation occurred heterogeneously, i.e., at the carbonate-melt interface, and homogeneously, i.e., within the melt. Heterogeneous nucleation also occurred on other available nucleation surfaces, such as microlites even at very low degrees of oversaturation (cf. Masotta et al. 2014) and probably explains the formation of small vesicles in crystal-rich domains (Figure 2d). Homogeneous nucleation in certain melt domains, in turn, implies that volatiles were added (likely by diffusion) and that volatile saturation was then locally achieved (cf. Hurwitz and Navon 1994).

Indeed, Ca-rich glass and vesicles are present in all 0 s experiments, with the Vesuvius experiments representing the most extreme case wherein the carbonate was completely dissolved at 0 s. Comparing (i) the Merapi dry series, wherein carbonate assimilation

required 300 s to reach an advanced stage and (ii) the Merapi wet series, wherein the carbonate was largely dissolved by 90 s, it becomes apparent that compositionally-controlled melt viscosity exerts a key control on the reaction rate.

For example, at 1200 °C, the Merapi dry, Merapi wet, and Vesuvius wet experiment starting materials (equivalent to the Ca-normal domains) have viscosities of $10^{2.7}$, $10^{1.4}$ and $10^{1.1}$ Pa.s, respectively (calculated after Giordano et al. 2008). If we take microcrystals in in the Merapi dry series into account, we obtain a viscosity value of $10^{3.5}$ Pa.s. On the other hand, the Ca-rich melts have calculated viscosities between $10^{0.3}$ and $10^{0.2}$ Pa.s for the Merapi and Vesuvius series, respectively (assuming 25 wt. % CaO), which is an order of magnitude lower than the results for the Ca-normal melts and confirms that the rate of carbonate dissolution is inversely related to melt viscosity.

In addition, the spatial distribution of vesicles in our time lapse experiments provides a record of bubble growth and migration. For all experiments, bubbles tend to move away from the carbonate clast as run time proceeds, with greater vesicle mobility in lower viscosity systems (Figure 8 and 9). Bubbles migrate away from the carbonate clast because a pressure and composition gradient is rapidly established in the experiments once the decarbonation reaction begins. The experiments quickly become oversaturated with CO_2 close to the reaction site and bubble nucleation and migration become the main mass transport mechanisms. In the experiments, fluid pressure is greater at the reaction site than in the distal parts of the capsule, which causes bubbles to move away from the reaction site in a broadly radial fashion (Figure 8 and 9). Importantly, throughout the whole Vesuvius series, larger bubbles tend to be positioned preferentially at the capsule margins (Figure 2 i-l), reflecting fast volatile migration into the uncontaminated areas. Vesicle migration is sluggish in more viscous systems, however. For instance, in the Merapi dry series, where bubbles and Ca-rich melt remain relatively close to the carbonate clast and/or the reaction site even at 300 s, virtually all bubbles are contained in the Ca-rich melt (Figure 2 d).

Conversely, bubbles occur in both the Ca-rich and Ca-normal melt in the Merapi wet series and there, the Ca-rich glass area is much wider. Notably, in the Merapi wet series, the boundary between Ca-rich and Ca-normal glasses follows the profile of large bubbles (Figure 2 f) or is aligned with many smaller bubbles (Figure 2 h and 4 b).

In the Vesuvius wet 0 s experiment, mixing/physical mingling between the Ca-rich and the Ca-normal melts is indicated by chemical gradients across the interface between the two glass domains. The interfaces between Ca-rich and Ca-normal melts roughly follow the shape of the bubbles, indicating that bubble migration facilitates melt mingling (Figure 2 and 5). We therefore suggest that the viscosity contrast between the Ca-rich and Ca-normal melts (see calculated values above) probably represents an initial hindrance for bubble migration and magma mixing, temporarily locking the bubbles in the Ca-rich melt as evident from the concentration of small bubbles along the contamination front in the Merapi dry series (Figure 3 b). In contrast, in the Merapi wet series, vesicles also grew in the Ca-normal zones. In this case, CO_2 pulsing from the carbonate resulted in CO_2 and bubble migration from the Ca-rich melt, as suggested by bubble trails in the Ca-normal glass that parallel the contamination front (e.g. Merapi wet 300 s; Figure 4 b). For the Vesuvius wet series, bubble nucleation also occurred in both Ca-rich and Ca-normal melts. The relatively low viscosity contrast between these two melts appears to have promoted rapid bubble migration and efficient CO_2 diffusion into the Ca-normal domains (Figure 5 b).

Prolonged nucleation dominates the Merapi dry and wet runs where both small and large bubbles increase in number with time (Figure 6 a, b). The similar cumulative vesicle number for Merapi wet 60 s and Vesuvius wet 0 s experiments (Figure 6), together with the increasing cumulative vesicle volume at longer run times for both Merapi series (not observed in Vesuvius experiments; Figure 7), demonstrates the different rates of assimilation-induced CO_2 exsolution. The slower assimilation rate causes prolonged

bubble nucleation in both the Merapi dry and wet series, relative to the Vesuvius wet series where nucleation is already exhausted as the carbonate is fully dissolved.

Fast digestion of carbonate in both Merapi and Vesuvius wet experiments hence causes sudden release of volatiles from the reaction site but ambient melt viscosity controls their migration style. Bubble release likely occurs in a pulsatory fashion as multiple vesiculation events (or "bubble blow-outs") are recognised from the sharp increases in vesicle number over a given diameter range in all of our experimental series (Figure 6). In fact, the number of vesiculation pulses increases with experimental duration, and for example, the Vesuvius and Merapi wet experiments record two vesiculation pulses at 0 s, but three are seen at 300 s (see Figure 6 b and c). Although evidence of coalescence is found in all experimental series, in the form of, e.g., partially retracted bubble walls and films (e.g. Merapi dry series; Figure 3 b), coalescence becomes the dominant growth mechanism in the low viscosity Vesuvius runs, where the overall number of bubbles (especially in the small size fraction) decreases with time (Figure 6 c).

Chemical gradients and "pile-up" of Ca and Sr between the Ca-rich and Ca-normal glass domains are found in both Merapi and Vesuvius hydrated experiments (Deegan et al. 2010; Jolis et al. 2013) and are of similar magnitude in all experiments (except for Vesuvius wet 300 s where homogenisation becomes increasingly relevant). The alignment of bubbles, both at and parallel to the contamination front, indicates a similar pile-up for CO_2, and underlines that volatile migration is influenced by viscosity through slowing down diffusive volatile migration and the movement of bubbles that have already formed.

Bubble formation affects both Ca-rich and Ca-normal domains, indicating that some CO_2 can diffuse through the rheological barrier at the melt interface(s) (Figure 2). We also note that in low viscosity systems bubbles are efficiently transported away from the carbonate, causing a high frequency of bubble blowouts that can create a steady state dissolution system, analogous to an effervescent tablet in water that dissolves in very rapid

pulses, usually almost too fast for us to see. In high viscosity systems, in contrast, bubbles are initially locked in the melt close to the carbonate where they continue to grow, thus generating fluid overpressure and potentially episodic bubble blowout events. Initiation of a bubble blowout in such systems could be caused by several factors including, (i) the bubble number density gradient between the contaminated and normal melt, (ii) a progressive change of the chemical gradient, i.e., an increased tendency towards chemical homogenisation, or (iii) external factors such as earthquakes, dyking, or magma replenishments (e.g. Deegan et al. 2011; Troll et al. 2012).

6.3 Implications for natural volcanic systems

The experiments represent laboratory simulations of magma-carbonate interaction, a process that has been shown to occur at both Merapi and Vesuvius volcanoes (Fulignati et al. 2004b; Chadwick et al. 2007; Iacono Marziano et al. 2009; Dallai et al. 2011; Borisova et al. 2013). The experiments are particularly relevant because they mirror features found in natural rocks. Micro-analyses of calc-silicate xenoliths from Merapi, for example, have been shown to contain extremely CaO-enriched, sometimes glassy domains (up to 61 wt.% CaO, Deegan et al. 2010). At Vesuvius, Mg-rich olivine demonstrates elevated $\delta^{18}O$ values relative to typical, mantle-derived mafic magmas due to carbonate-derived CO_2 fluxing in the roots of the volcanic system (Dallai et al. 2011). While the isothermal conditions of the experiments may not be fully applicable to assimilation at magma chamber walls, i.e., with a strong thermal contrast (cf. Del Moro et al. 2001; Spera and Bohrson 2001), the experimental conditions replicate magmatic digestion of a stoped carbonate block or xenoliths from a "warm" chamber roof or wall (i.e. we assume the mass of the assimilated clast to be much less than that of the magma that provides heat to drive the reaction; Figure 9). Specifically, we found that melt viscosity exerts a major control on the carbonate dissolution reaction by regulating the efficiency of bubble migration from the reaction site,

which in turn determines how fast the carbonate can be digested. Low viscosity systems such as Vesuvius will likely permit frequent vesiculation pulses where bubbles can migrate freely from the Ca-rich melt. Efficient migration of bubbles from the dissolving carbonate can thus trigger more frequent new vesiculation pulses and promote higher assimilation rates (Figure 9). This style of vesiculation would lead to steady state CO_2-production for as long as the reactant is available. A potential outcome of this process would be an increase in the buoyancy of Vesuvius magmas that would trigger rapid ascent and lead to sustained explosive eruptions (cf. Dallai et al. 2011).

For a more viscous magma (e.g. Merapi), bubble accumulation at the reaction site will progressively retard the carbonate dissolution reaction and the magma will locally behave as a closed system. If bubbles are not transported away, the reaction will simultaneously increase local fluid pressure until it terminates due to a lack of melt at the reaction site. If the confining pressure is exceeded during this process, however, a bubble blow-out may be triggered in a broadly radial fashion from the reaction site, i.e., the carbonate (Figure 8 and 9), thus relieving localised fluid over-pressure and allowing the decarbonation reaction to proceed again. This type of vesiculation would lead to an explosive, gas-driven eruption once the overpressure threshold is exceeded and may be repeated with successive CO_2 build up events. This may apply to Merapi, especially the pre-2010 eruptions, as the latter was a "100-year event" (Surono et al. 2012) caused by a large contribution of fresh, low viscosity basaltic magma from depth, rather than a dome-forming eruption as typical of the 20^{th} century activity at Merapi. Notably, the bubble-blow out mechanism seems to be also recorded in plutonic systems that underwent magma-carbonate interaction, such as the Hortavaer intrusive complex, Norway, where fragmented structures have been interpreted in this context (Barnes et al. 2009).

Regardless of the vesiculation style presented by a magmatic system undergoing magma-carbonate interaction, a fundamental finding from the experiments is that CO_2

fluxing from carbonate is coupled to magma viscosity. Where vesiculation becomes progressively sluggish, the bubble blow-out mechanism described here can re-ignite vesiculation once the local fluid pressure threshold has been exceeded. In contrast, efficient CO_2 fluxing is permitted in relatively low viscosity melts, which will allow carbonate assimilation to proceed unhindered and will likely lead to steady-state degassing.

The wider implication arising from these observations is that carbonate assimilation in a variety of different types of magmatic systems with differing melt properties can nevertheless contribute substantial quantities of CO_2 to the atmosphere via volcanism. It is thus imperative that carbonate-rich upper crustal lithologies beneath arcs are considered in mass balance models concerning Earth's deep carbon-cycle (cf. Johnston et al. 2011; Troll et al. 2012; Dasgupta 2013; Lee et al. 2013).

Acknowledgements

Lucia Civetta is thanked for providing the samples for the Vesuvius experiments and Giovanni Orsi for discussion on Vesuvius magmatic processes. Claus Siebe, Ben van Wyk de Vries and Silvio Mollo are thanked for encouraging discussion on the experiments. We also thank Michael Heap and two anonymous reviewers for their constructive comments that helped to improve the manuscript and Jochen Hoefs for editorial handling. This work was supported by Istituto Nazionale di Geofisica e Vulcanologia (INGV), the Irish Research Council for Science, Engineering and Technology (IRCSET), the Center for Natural Disaster Studies (CNDS) at Uppsala University (UU), and by the Swedish Science Foundation (VR).

References

Abramoff MD, Magalhães PJ, Ram SJ (2004) Image processing with ImageJ. Biophotonics International 11:36-42.

Auger E, Gasparini P, Virieux J, Zollo A (2001) Seismic Evidence of an Extended Magmatic Sill Under Mt. Vesuvius. Science 294:1510-1512.

Barberi F, Bizouard H, Clocchiatti R, Metrich N, Santacroce R, Sbrana A (1981) The Somma-Vesuvius Magma Chamber: a Petrological and Volcanological Approach. Bull Volcanol 44:295-315.

Barnes CG, Prestvik T, Barnes MAW, Anthony EY, Allen CM (2003) Geology of a magma transfer zone: the Hortavær Igneous Complex, north-central Norway. Nor J Geol 83:187-208.

Barnes CG, Prestvik T, Sundvoll B, Surratt D (2005) Pervasive assimilation of carbonate and silicate rocks in the Hortavær igneous complex, north-central Norway. Lithos 80:179-199.

Barnes CG, Prestvik T, Li Y, McCulloch L, Yoshinobu AS, Frost CD (2009) Growth and zoning of the Hortavaer intrusive complex, a layered alkaline pluton in the Norwegian Caledonides. Geosphere 5, 286-301.

Borisova AY, Martel C, Gouy S, Pratomo I, Surmarti S, Toutain J-P, Bindeman IN, de Parseval P, Metaxian J-P, Surono (2013) Highly explosive 2010 Merapi eruption: Evidence for shallow-level crustal assimilation and hybrid fluid. J Volcanol Geotherm Res 261:193-208

Botcharnikov R, Freise M, Holtz F, Behrens H (2005) Solubility of C-O-H mixtures in natural melts: new experimental data and application range of recent models. Ann Geophys 48:633-646.

Botcharnikov RE, Behrens H, Holtz F (2006) Solubility and speciation of C-O-H fluids in andesitic melt at *T*=1100-1300 ºC and *P*=200 and 500 MPa. Chem Geol 229:125-143.

Bruno PPG, Cippitelli G, Rapolla A (1998) Seismic study of the Mesozoic carbonate basement around Mt. Somma-Vesuvius, Italy. J Volcanol Geotherm Res 84:311-322.

Camus G, Gourgaud A, Mossand-Berthommier P-C, Vincent P-M (2000) Merapi (Central Java, Indonesia): An outline of the structural and magmatological evolution, with a special emphasis to the major pyroclastic events. J Volcanol Geotherm Res 100:139-163.

Chadwick JP, Troll VR, Ginibre C, Morgan D, Gertisser R, Waight TE, Davidson JP (2007) Carbonate assimilation at Merapi Volcano, Java, Indonesia: Insights from Crystal Isotope Stratigraphy. J Petrol 48:1793-1812.

Chadwick JP, Troll VR, Waight TE, van der Zwan FM, Schwarzkopf LM (2013) Petrology and geochemistry of igneous inclusion in recent Merapi deposits: a window into the sub-volcanic plumbing system . Contrib Mineral. Petrol. 165:259-282.

Civetta L, D'Antonio M, de Lorenzo S, De Renzo V, Gasparini P (2004) Thermal and geochemical constraints on the 'deep' magmatic structure of Mt. Vesuvius. J Volcanol Geotherm Res 113:1-12.

Curray JR, Shor Jr GG, Raitt RW, Henry M (1977) Seismic Refraction and Reflection Studies of Crustal Structure of the Eastern Sunda and Western Banda Arcs. J Geophys Res 82: 2479-2489.

Dasgupta R (2013) Ingassing, storage, and outgassing of terrestrial carbon through geological time. Rev Mineral Geochem 75:183-229.

Dallai L, Cioni R, Boschi C, D'Oriano C (2011) Carbonate-derived CO_2 purging magma at depth: Influence on the eruptive activity of Somma-Vesuvius, Italy. Earth Planet Sci Lett 310: 84-95.

Deegan FM, Troll VR, Freda C, Misiti V, Chadwick JP, McLeod CL, Davidson JP (2010) Magma-Carbonate Interaction Processes and Associated CO_2 release at Merapi Volcano, Indonesia: Insights from Experimental Petrology. J Petrol 51:1027-1051.

Del Moro A, Fulignati P, Marianelli P, Sbrana A (2001) Magma contamination by direct wall rock interaction: constraints from xenoliths from the walls of a carbonate-hosted magma chamber (Vesuvius 1944 eruption). J Volcanol Geotherm Res 112:15-24.

Dixon JE (1997) Degassing of alkali basalts. Am Miner 82:368-378.

Freda C, Gaeta M, Palladino DM, Trigila R (1997) The Villa Senni Eruption (Alban Hills, central Italy): the role of H_2O and CO_2 on the magma chamber evolution and on the eruptive scenario. J Volcanol Geotherm Res 78:103–120

Freda C, Gaeta M, Misiti V, Mollo S, Dolfi D, Scarlato P (2008) Magma-carbonate interaction: an experimental study on ultrapotassic rocks from Alban Hills (Central Italy). Lithos 101:397-415.

Freda C, Gaeta M, Giaccio B, Marra F, Palladino DM, Scarlato P, Sottili G (2011) CO_2-driven large mafic explosive eruptions: the Pozzolane Rosse case study from the Colli Albani Volcanic District (Italy). Bull Volcanol 73:241-256.

Fulignati P, Marianelli P, Santacroce R, Sbrana A (2000) The skarn shell of the 1944 Vesuvius magma chamber. Genesis and P-T-X conditions from melt and fluid inclusion data. Eur J Mineral 12:1025-1039

Fulignati P, Marianelli P, Santacroce R, Sbrana A (2004a) Probing the Vesuvius magma chamber-host rock interface through xenoliths. Geol Mag 151:417-428

Fulignati P, Marianelli P, Métrich N, Santacroce R, Sbrana A (2004b) Towards a reconstruction of the magmatic feeding system of the 1944 eruption of Vesuvius. J Volcanol Geotherm Res 133:13-22.

Gaeta M, Di Rocco T, Freda C (2009) Carbonate Assimilation in Open Magmatic Systems: the Role of Melt-bearing Skarns and Cumulate-forming Processes. J Petrol 50:361-385.

Ganino C, Arndt NT (2009) Climate changes caused by degassing of sediments during the emplacement of large igneous provinces. Geology 37:323-326.

Gardner, JE, Hilton, M & Carroll, M R (1999) Experimental constraints on degassing of magma: Isothermal bubble growth during continuous decompression from high pressure. Earth Planet Sci Lett 122168: 201-218.

Gertisser R, Keller J (2003) Trace Element and Sr, Nd, Pb and O Isotope Variations in Medium-K and High-K Volcanic Rocks from Merapi Volcano, Central Java, Indonesia: Evidence for the Involvement of Subducted Sediments in Sunda Arc Magma Genesis. J Petrol 44:457-489.

Giordano D, Russell JK, Dingwell DB (2008) Viscosity of magmatic liquids: A model. Earth Planet Sci Lett 271:123-134.

Goff F, Love SP, Warren RG, Counce D, Obenholzner J, Siebe C, Schmidt SC (2001) Passive infrared remote sensing evidence for large, intermittent CO emissions at Popocatépetl volcano, Mexico. Chem Geol 177:133-156.

Graham DW, Allard P, Kilburn CRJ, Spera FJ, Lupton JE (1993) Helium isotopes in some historical lavas from Mount Vesuvius. J Volcanol Geotherm Res 58:359-366.

Hamilton W (1979) Tectonics of the Indonesian Region. USGS Prof Pap 1078:1-345.

Heap MJ, Mollo S, Vinciguerra S, Lavallée Y, Hess K-U, Dingwell DB, Baud P, Iezzi G (2013) Thermal weakening of the carbonate basement under Mt. Etna volcano (Italy): implications for volcano instability. J Volcanol Geotherm Res 250:42-60.

Heap MJ, Lavallée Y, Petrakova L, Baud P, Reuschlé T, Varley N, Dingwell DB (2014) Microstructural controls on the physical and mechanical properties of edifice-forming andesites at Volcán de Colima, Mexico. J Volcanol Geotherm Res 119:2925-2963.

Holloway JR, Blank JG (1994) Application of experimental results to C-O-H species in natural melts. In: Carroll MR, Holloway JR (eds) Volatiles in Magmas. Rev Miner 30:187-230.

Hurwitz S Navon O (1994) Bubble nucleation in rhyolitic melts: Experiments at high pressure, temperature and water content. Earth Planet Sci Lett 122:267-280.

Iacono Marziano G, Gaillard F, Scaillet B, Pichavant M, Giovanni C (2009). Role of non-mantle CO_2 in the dynamics of volcano degassing: The Mount Vesuvius example. Geology 37:319-322.

Johnston FKB, Turchyn AV (2011) Edmonds, M. Decarbonation efficiency in subduction zones: Implications for warm Cretaceous climates. Earth Plan Sci Lett 303:143-152.

Jolis EM, Freda C, Troll VR, Deegan FM, Blythe LS, McLeod C, Davidson JP (2013) Experimental simulation of magma-carbonate interaction beneath Mt. Vesuvius, Italy. Contrib Mineral and Petrol 166:1335-1353.

Kerrick DM, Connolly JAD (2001) Metamorphic devolatilization of subducted marine sediments and the transport of volatiles into the Earth's mantle. Nature 411:293-296.

Lee CTA, Shen B, Slotnick BS, Liao K, Dickens GR, Yookoyama Y, Lenardic A, Dasgupta R, Jellinek M, Lackey JS, Schneider T, Tice MM (2013) Continental arc-island arc fluctuations, growth of crustal carbonates, and long-term climate change. Geosphere 9:21-36.

Martelli M, Nuccio PM, Stuart FM, Burgess R, Ellam RM, Italiano F (2004) Helium-strontium isotope constraints on mantle evolution beneath the Roman Comagmatic Province, Italy. Earth Planet Sci Lett 224:295-308.

Masotta, M., Ni, H., Keppler, H. (2014) In situ observations of bubble growth in basaltic, andesitic and rhyodacitic melts. Contrib Mineral and Petrol 167:976. doi: 10.1007/s00410-014-0976-8.

Mollo S, Gaeta M, Freda C, Di Rocco T, Misiti V, Scarlato P (2010) Carbonate assimilation in magmas: A reappraisal based on experimental petrology. Lithos 114:503-514.

Mollo, S., Heap, M.J., Iezzi, G., Hess, K.-U., Scarlato, P., Dingwell, D.B., 2012. Volcanic edifice weakening via decarbonation: a self-limiting process? Geophys Res Lett 36, L15307. http://dx.doi.org/10.1029/2012GL052613.

Papale P, Moretti R, Barbato D (2006) The compositional dependence of the saturation surface of $H_2O + CO_2$ fluids in silicate melts. Chem Geol 229:78-95.

Peccerillo A (2005) Plio-Quaternary Volcanism in Italy. Petrology, Geochemistry, Geodynamics. Springer, Berlin. Pp 129-171.

Sahagian DL, Proussevitch AA (1998) 3D particle size distributions from 2D observations: stereology for natural applications. J Volcanol Geotherm Res 84:173-196.

Scaillet B, Pichavant M, Cioni R (2008) Upward migration of Vesuvius magma chamber over the past 20,000 years. Nature 455:216-220.

Schaaf P, Stimac J, Siebe C, Macías JL (2005) Geochemical evidence for mantle origin and crustal processes in volcanic rocks from Popocatépetl and surrounding monogenetic volcanoes, Central Mexico. J Petrol 46:1243-1282.

Shea T, Houghton BF, Gurioli L, Cashman KV, Hammer JE, Hobden BJ (2010) Textural studies of vesicles in volcanic rocks: an integrated methodology. J Volcanol Geotherm Res 190:271-289.

Smyth H, Hall R, Hamilton J. Kinny P (2005) East Java: Cenozoic basins, volcanoes and ancient basement. In: Proceedings, Indonesian Petroleum Association Thirtieth Annual Convention & Exhibition, August 2005. IPA05-G-045.

Spera FJ, Bohrson WA (2001) Energy-Constrained Open-System Magmatic Processes I: General Model and Energy Constrained Assimilation and Fractional Crystallisation (EC-AFC) Formulation. J Petrol 42:999-118.

Surono, Jousset P, Pallister J, Boichu M, Fabrizia Buongiorno M, Budisantoso A, Costa F, Andreastuti S, Prata F, Schneider D, Clarisse L, Humaida H, Sumarti S, Bignami C,

Griswold J, Carn S, Oppenheimer C, Lavigne F (2012) The 2010 explosive eruption of Java's Merapi volcano – a '100-year' event. J Volcanol Geotherm Res 241:121-135.

Svensen H, Planke S, Polozov AG, Schmidbauer N, Corfu F, Podladchikov YY, Jamtveit B (2009) Siberian gas venting and the end-Permian environmental crisis. Earth Plan Sci Lett 277:490-500.

Tregoning P, Brunner FK, Bock Y, Puntodewo SSO, McCaffrey R, Genrich JF, Calais E, Rais J, Subarya C (1994) First geodetic measurement of convergence across the Java Trench. Geophys Res Lett 21:2135-2138.

Troll, VR, Hilton, DR, Jolis, EM, Chadwick, JP, Blythe, LS, Deegan, FM, Schwarzkopf, LM, Zimmer, M (2012) Crustal CO_2 liberation during the 2006 eruption and earthquake events at Merapi volcano, Indonesia. *Geophys*. *Res*. *Lett*. 39, L11302, doi: 10.1029/2012GL051307.

Troll, VR, Deegan, FM, Jolis, EM, Harris, C, Chadwick, JP, Gertisser, R, Schwarkopf, LM, Borisova, AY, Bindeman, IN, Sumarti, S, Preece, K (2013) Magmatic differentiation processes at Merapi volcano: inclusion petrology and oxygen isotopes. J. Volcanol. Geotherm. Res., 261:38-49.

Troll, VR, Deegan, FM, Jolis, EM, Budd, DA, Dahren, B., Schwarzkopf, LM (2015) Ancient oral tradition describes volcano-earthquake interaction at Merapi volcano, Indonesia. Geografiska Annaler, 97:137-166.

van Bemmelen RW (1949) The geology of Indonesia. Government Printing Office, The Hague. Pp 1-732.

van der Zwan F, Chadwick JP, Troll VR (2013) Textural history of recent basaltic-andesites and plutonic inclusions from Merapi volcano. Contrib Mineral Petrol 166:43-63.

Vetere F, Botcharnikov RE, Holtz F, Behrens H, De Rosa R (2011) Solubility of H_2O and CO_2 in shoshonitic melts at 1250 ºC and pressures from 50 to 400 Mpa: Implications for Campi Flegrei magmatic systems. J Volcanol Geotherm Res 202:251-261.

Watkinson DH, Wyllie PJ (1964) The limestone assimilation hypothesis. Nature 204:1053-1054.

Watkinson DH, Wyllie PJ (1969) Phase equilibrium studies bearing on the limestone-assimilation hypothesis. Geol Soc Am Bull 80:1565-1576

Werner C, Brantley S (2003) CO_2 emissions from the Yellowstone volcanic system. Geochem Geophys Geosys 4:1061, doi:10.1029/2002GC000473.

Zollo A, Gasparini P, Virieux J, le Meur H, de Natale G, Biella G, Boschi E, Capuano P, de Franco R, dell'Aversana P, de Matteis R, Guerra I, lannaccone G, Mirabile L, Vilardo G (1996) Seismic Evidence for a Low-Velocity Zone in the Upper Crust Beneath Mount Vesuvius. Science 274:592-594.

Figure Captions

Fig 1 Heywood diameter vs corrected cumulative number (C_{CORR}) of vesicles for Vesuvius wet 0 s experiment. The cumulative vesicle correction extrapolates the number of vesicles measured over the area of the whole capsule. The data are firstly divided into respective magnification groups at which the vesicles were measured. Subsequently, the most representative magnification group for vesicles of different diameters was identified. The 0-80 magnification group is most representative of, e.g., the largest vesicles, characterising those to ca. 16 μm in size, while the other curves are more representative of smaller sizes. A complete experimental curve can thus be reconstructed from the individual magnification curves (see Fig 6c).

Fig 2 Back-scatter electron images of textures and vesicle distributions produced in the three different experimental series and at four experimental durations. **a)** to **d)** Merapi dry series; **e)** to **h)** Merapi wet series; and **i)** to **l)** Vesuvius wet series. Annotations show the remnant carbonate, the Ca-normal and crystal-rich domain, the Ca-rich glass and, where appropriate, the contamination front.

Fig 3 Merapi dry 60 s experiment **a)**. Vesicles form at the interface between melt and carbonate (the reaction site). Smaller vesicles are generally located closer to the carbonate remnant. The contamination front, at the interface between the Ca-rich and the Ca-normal glasses, contours the outside edge of the larger vesicles. This suggests that bubble growth and bubble migration plays a role in driving the contamination process in lower viscosity systems. **b)** Merapi dry 300 s experiment. Smaller vesicles collect at the contamination front between the crystal-rich domain and the Ca-normal glass. Two large vesicles can be seen to coalesce on the right hand side of the image. Both quench crystals and smaller

vesicles are present in the crystal-rich domain, while there are almost no small vesicles or crystals in the Ca-rich glass.

Fig 4 Merapi wet 60 s experiment. **a)** Example of dendritic texture present in some samples. This texture results from quenching of the Ca-rich melt that has digested calcite. Vesicles are located near the edge of the carbonate clast, some surrounded by microcrystals of calcite. **b)** Merapi wet 300s experiment. Vesicles of similar size are aligned parallel to the contamination front, but are located ahead of it in the Ca-normal glass. The lower viscosity of the Merapi wet experiments relative to the Merapi dry ones allows volatiles to diffuse away from the reaction site more quickly. Here, all volatiles produced in one single vesiculation event seem to move away perpendicular to the reaction site at a similar rate. However, the viscosity is still relatively high in the Merapi wet series and substantial mingling between the Ca-rich and Ca-normal melts is not yet observed in this experimental series.

Fig 5 Vesuvius wet 0 s experiment. **a)** At 0 s, just as experimental temperature is reached, intermingling of Ca-rich and Ca-normal glass has already commenced, causing complex textures in comparison to the Merapi dry and wet series. Smaller vesicles in the Ca-normal glass align themselves along the contamination front (CF). Beyond the CF, i.e., further into the Ca-normal glass, smaller vesicles occur, but do not form a regular pattern (e.g. Figure 4b). The black line around the dendritic textured area highlights the location of the higher magnification image shown in Figure 5b. **b)** The dendritic texture demonstrates a strong CaO enrichment but is not associated with any solid carbonate remnants.

Fig 6 Cumulative vesicle correction (C_{CORR}) vs vesicle diameter (μm) for **a)** Merapi dry, **b)** Merapi wet, and **c)** Vesuvius wet experiments. All four experiment durations (0 s, 60 s, 90

s and 300 s) are plotted. The number of vesiculation events that can be identified increases from two in the Merapi wet 0 s to three in the Merapi wet 300 s. A similar sequence of events is also observed in the Vesuvius wet experiments. Vesicle coalescence can be identified where the number of bubbles in the smaller size fraction decreases with longer experimental duration (compare Figure 7c).

Fig 7 Cumulative vesicle volume (C_{VOL} μm^3) vs vesicle diameter (μm) for **a)** Merapi dry, **b)** Merapi wet, and **c)** Vesuvius wet experiments. All four experiment durations (0 s, 60 s, 90 s and 300 s) are plotted. For **a)** and **b)** as experiment duration increases from 0 s to 300 s, a general increase in the cumulative volume of bubbles is observed, demonstrating that decarbonation has not reached completion in the shorter duration runs, and that more CO_2 is exsolved in the longer duration experiments as the reaction proceeds. In **c)**, the cumulative volume of vesicles is the same for all experimental durations. This indicates that by 0 s (i.e. just as experimental temperatures are reached) the decarbonation reaction is almost complete. As experimental duration increases for this series, homogenisation of the reaction products is the only change observed, i.e., no new bubbles are generated.

Fig 8 Schematic diagram of carbonate dissolution processes. **a)** Start of carbonate dissolution. Bubbles nucleate mostly in the Ca-rich melt close to the dissolving carbonate fragment, although some appear also in the Ca-normal melt. **b)** The carbonate clast decreases in size, and the Ca-rich melt increases in volume. Larger vesicles grow by diffusion and coalescence, pushing earlier bubbles and the contamination front away from the carbonate clast. Small vesicles parallel the contamination front, but are also found in Ca-normal melt where they formed as a result of volatile diffusion beyond the contamination front (Merapi wet and Vesuvius cases). Stages **a)** and **b)** will be repeated multiple times as the carbonate clast dissolves in vesiculation pulses. The frequency and

867 style of these pulses is controlled by the rate of removal of dissolved and exsolved CO_2
868 from the reaction site, which itself is controlled by melt viscosity. Once CO_2 has migrated
869 from the reaction site, dissolution can proceed further, thus allowing for the next
870 vesiculation pulse. **c)** Eventually, the whole carbonate clast dissolves, and the majority of
871 smaller bubbles coalesce into a small number of larger ones. Most vesicles have moved
872 away from the centre reaction site and bubble growth and migration promotes significant
873 mingling and mixing of melts.
874
875 **Fig 9** Model depicting magma-carbonate interaction processes prior to an eruption. **a)** The
876 plumbing systems beneath both Vesuvius and Merapi consist of magma pockets distributed
877 through the crust, which provide ample surface area for extensive magma-crust interaction.
878 **b)** Carbonate xenoliths are entrained into a slowly crystallising pocket of magma through,
879 e.g., stoping, dyking, or earthquake activity. Reaction between carbonate blocks and the
880 surrounding host melt produces CO_2 bubbles and a contaminated Ca-rich melt. The
881 reaction area is initially localised and confined to the proximity of the carbonate. **c)** As the
882 reaction continues, multiple vesiculation pulses cause CO_2 to penetrate a larger volume of
883 host melt. Vesicle growth, coalescence, and migration thus promote mingling of Ca-rich
884 and Ca-normal melts. If melt viscosity is relatively high (e.g. Merapi), volatiles are unable
885 to freely escape and localised over-pressurisation can be achieved, resulting in an
886 explosive "bubble blowout" event. Alternatively, if melt viscosity is relatively low (e.g.
887 Vesuvius), efficient removal of CO_2 bubbles allows for a higher reaction rate, which
888 results in more sustained volatile escape.
889

Figure 1
Click here to download Figure: Blythe_Fig 1_UPLOAD.tif

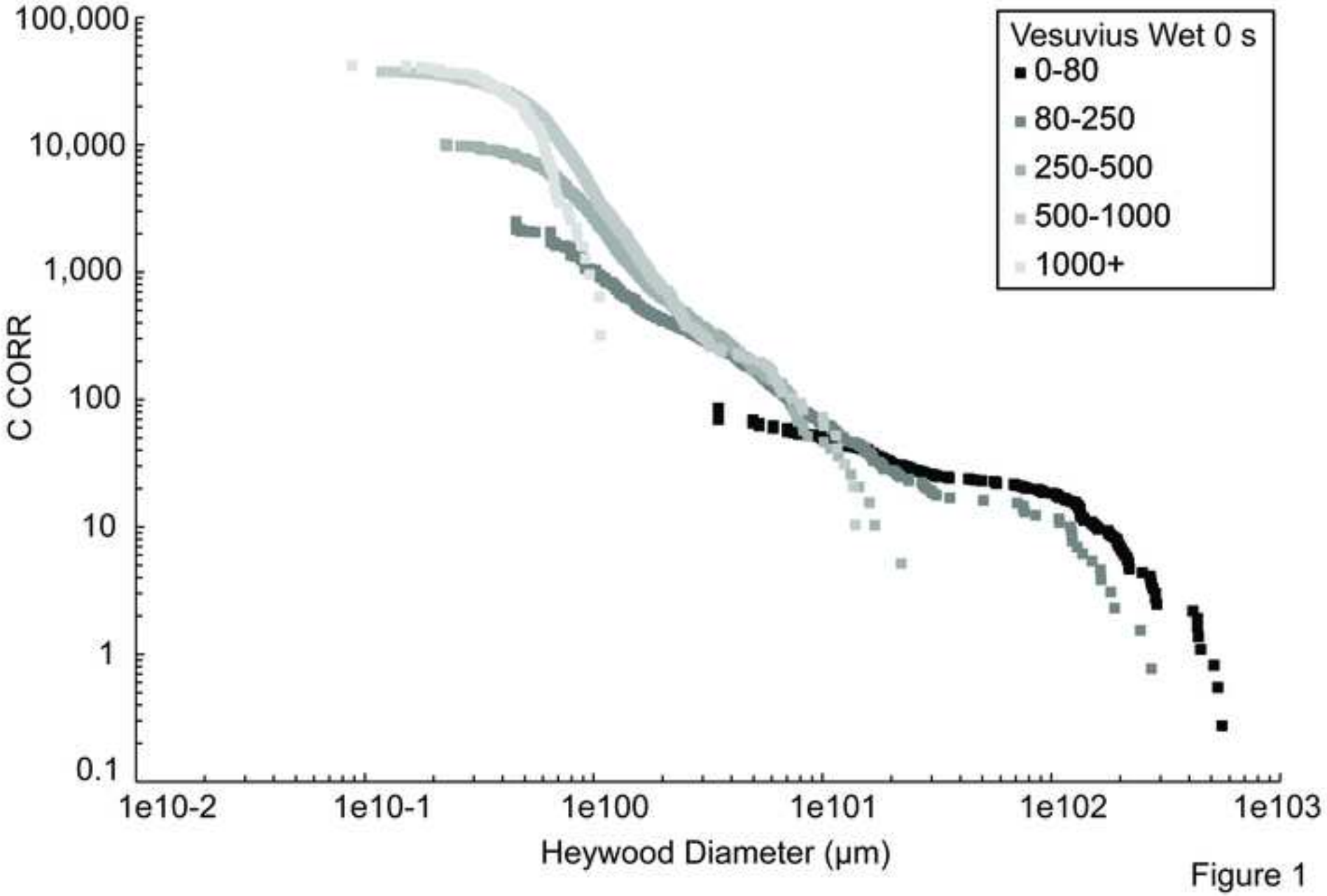

Figure 1

Figure 2

Click here to download Figure: Blythe_Fig 2_UPLOAD.tif

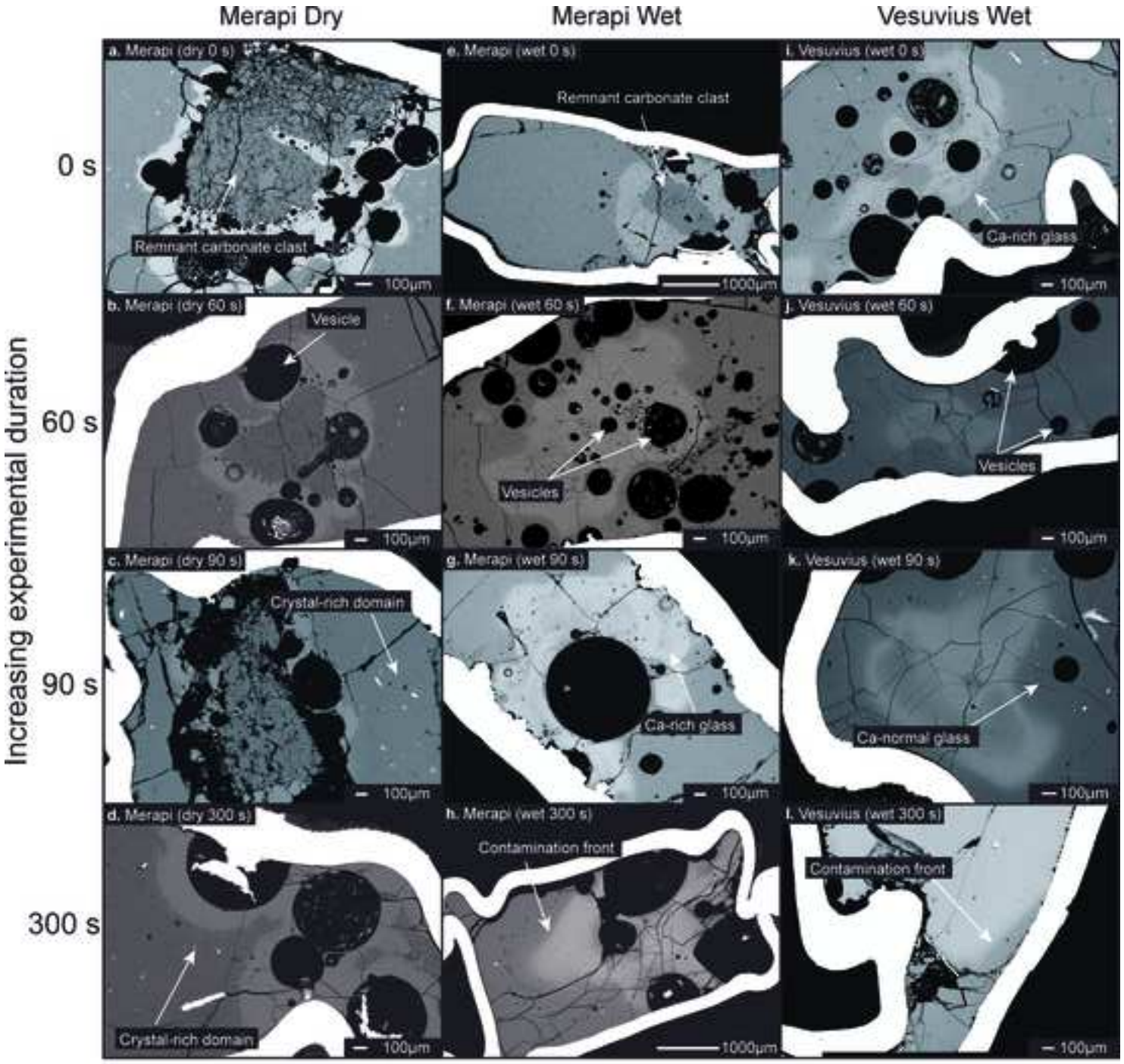

Figure 2

Figure 3
Click here to download Figure: Blythe_Fig 3_UPLOAD.tif

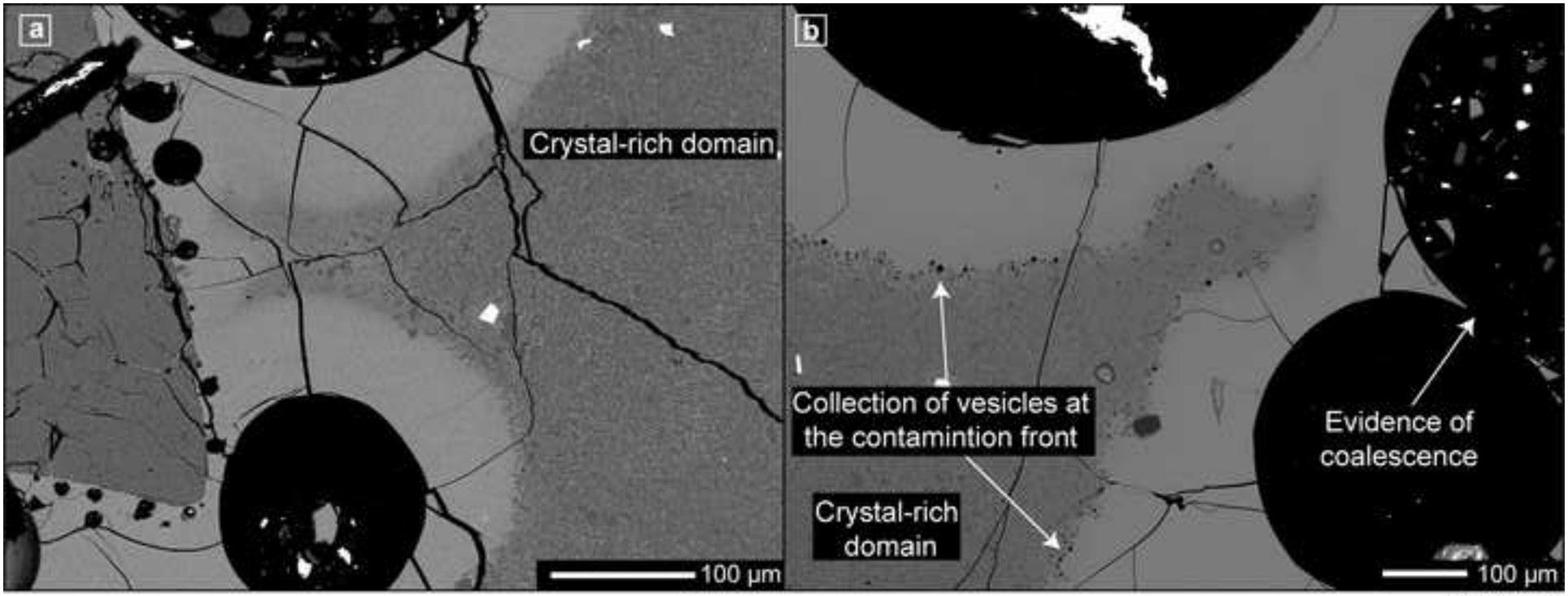

Figure 3

Figure 4
Click here to download Figure: Blythe_Fig 4_UPLOAD.tif

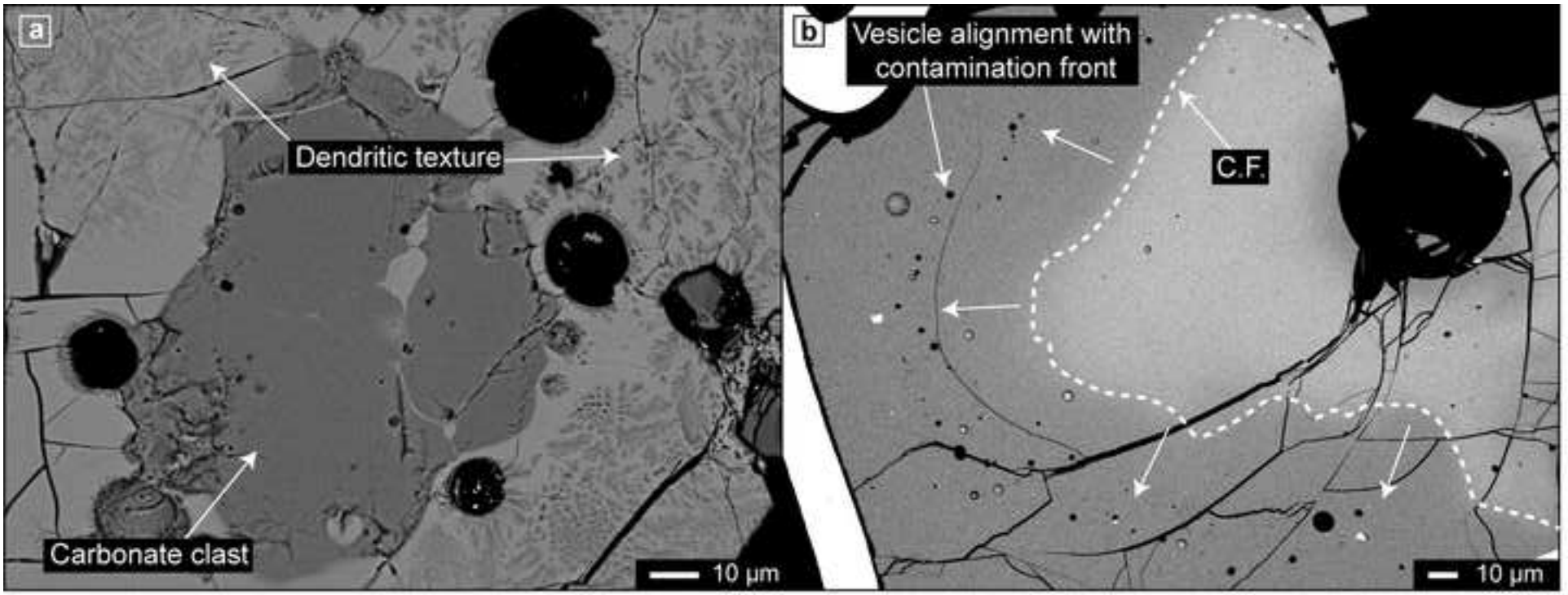

Figure 4

Figure 5
Click here to download Figure: Blythe_Fig 5_UPLOAD.tif

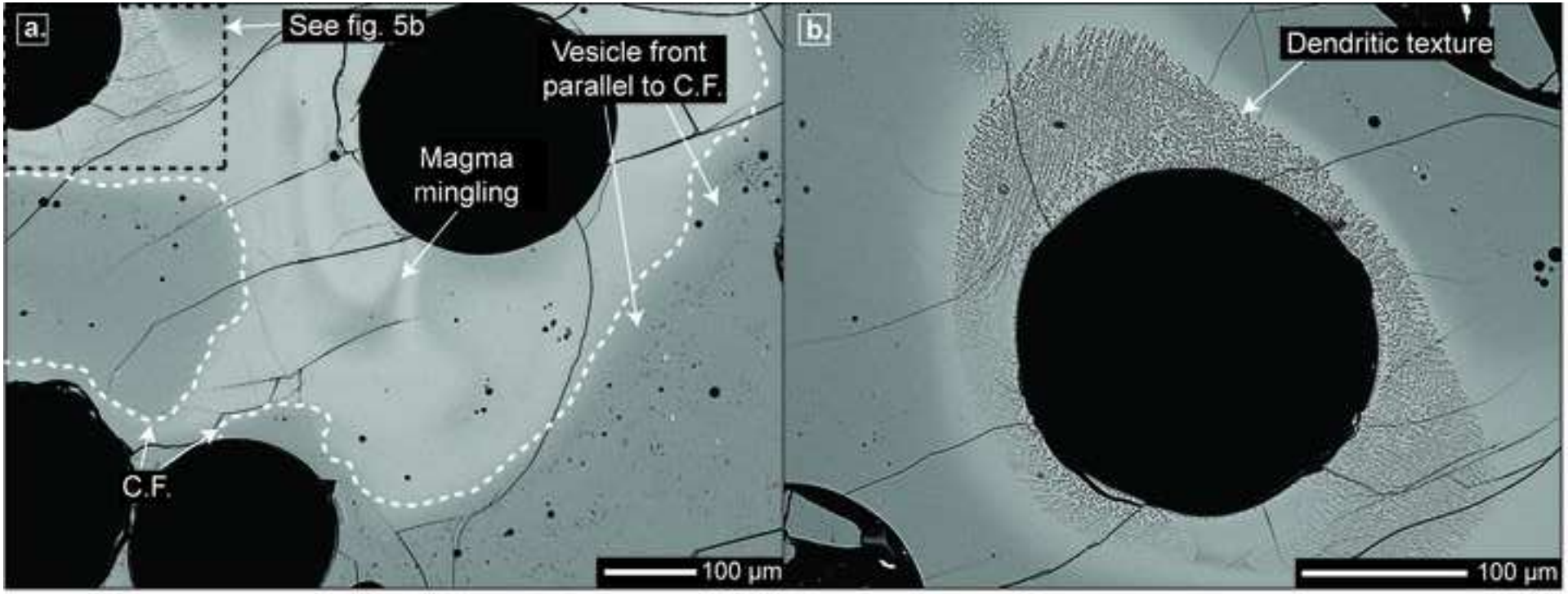

Figure 5

Figure 6

Click here to download Figure: Blythe_Fig 6_UPLOAD.tif

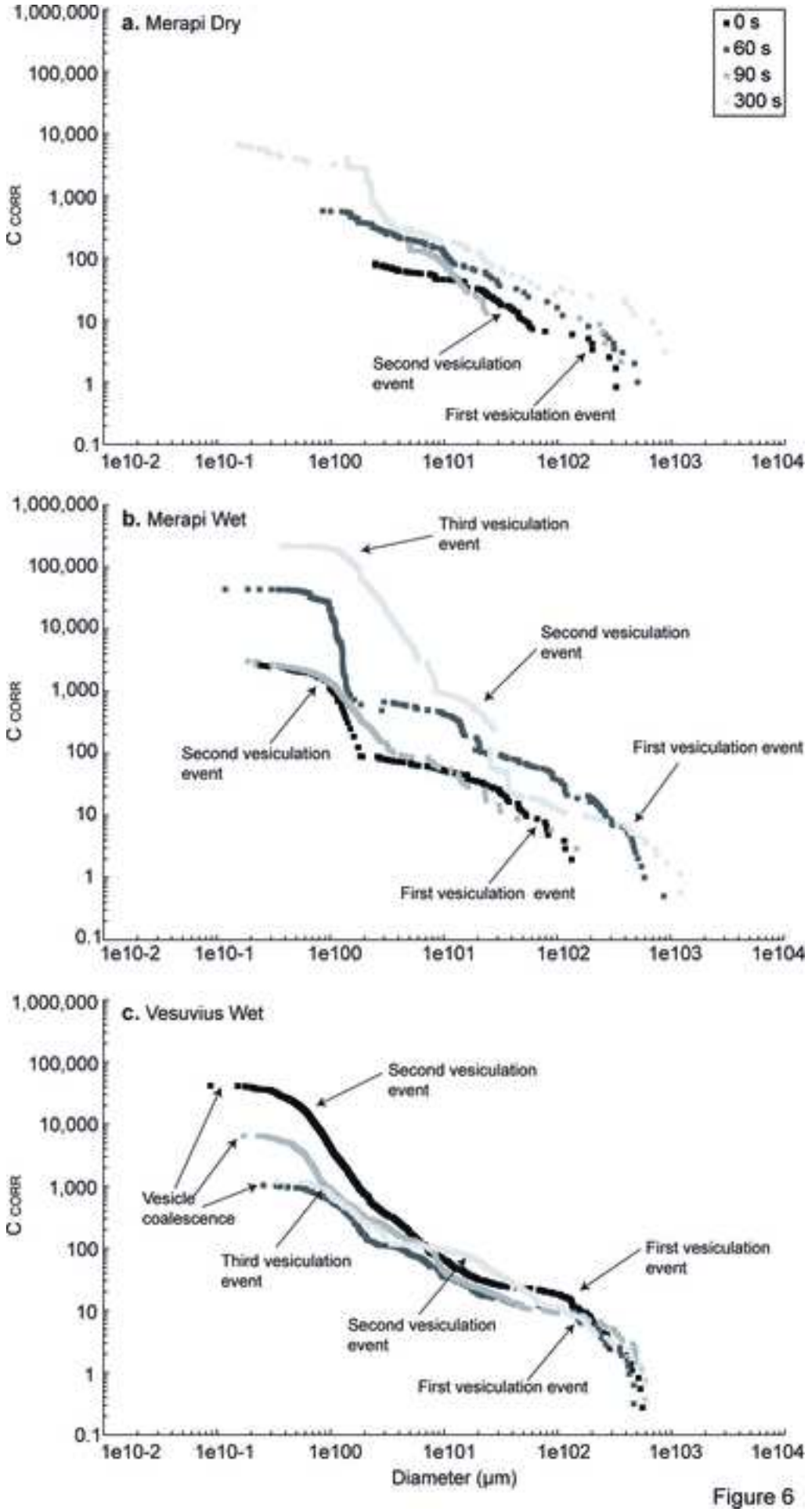

Figure 6

Figure 7

Click here to download Figure: Blythe_Fig 7_UPLOAD.tif

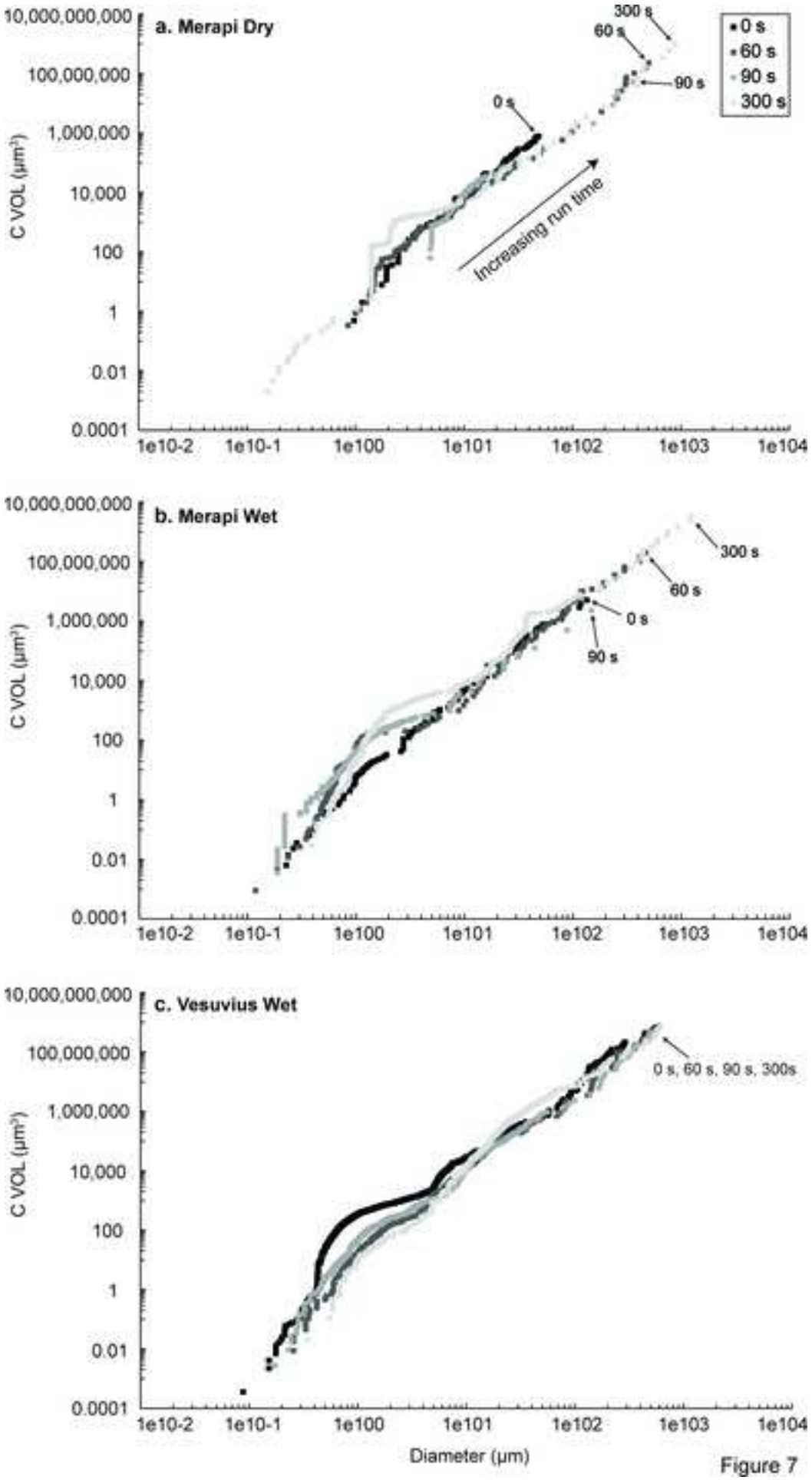

Figure 7

Figure 8
Click here to download Figure: Blythe_Fig 8_141009_UPLOAD.tif

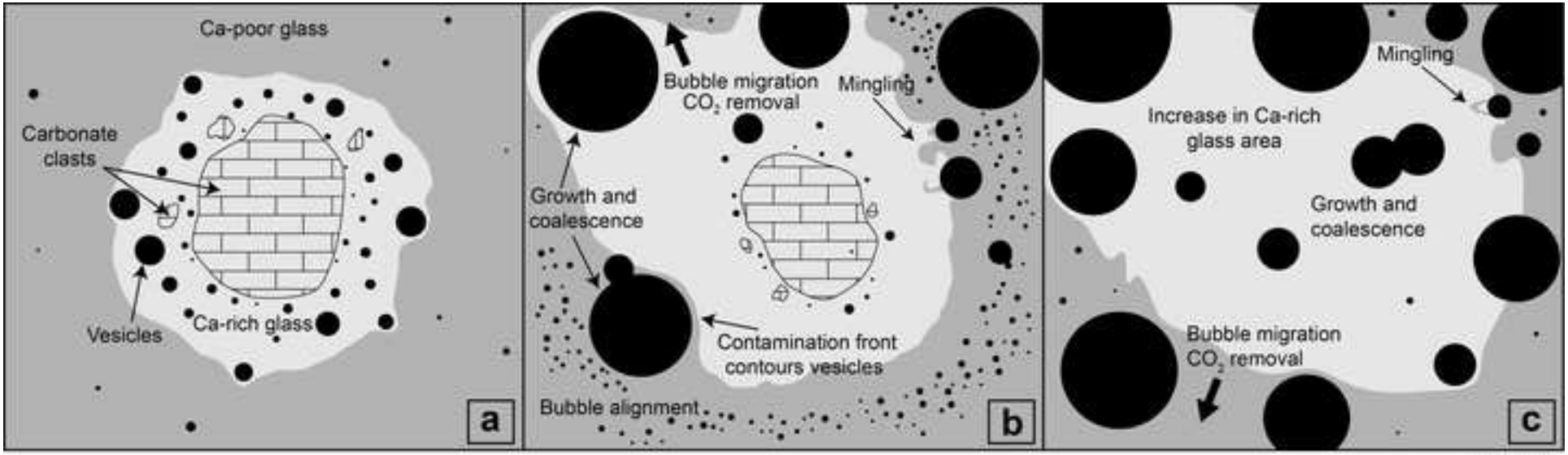

Figure 8

Figure 9
Click here to download Figure: Blythe_Fig 9_150325_UPLOAD.tif

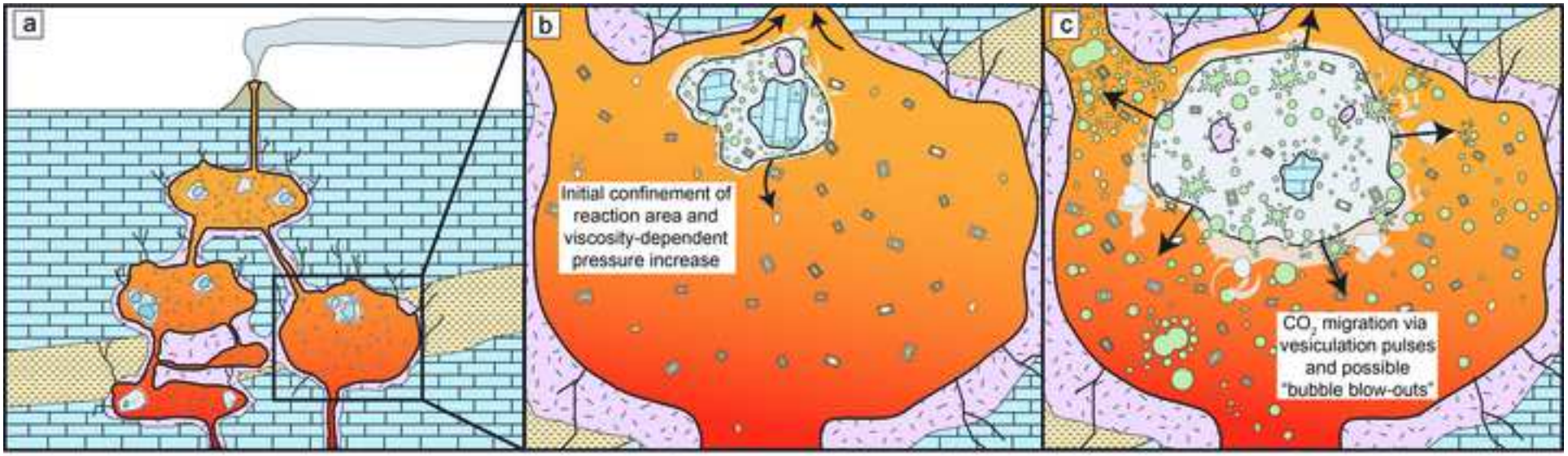

Figure 9

Table 1
Click here to download Table: Blythe et al_Table 1_UPLOAD.doc

Table 1. *Experimental conditions used for each series*

Run[1,2]	Starting Material	H_2O (wt. %)	Carbonate (wt. %)[3]	T (°C)	P (MPa)	t (s)
Merapi Dry Series[1]						
379-16	Basaltic-Andesite	0	19.6	1200	500	0
387-20	Basaltic-Andesite	0	20.0	1200	500	60
376-10	Basaltic-Andesite	0	19.0	1200	500	90
386-18	Basaltic-Andesite	0	19.4	1200	500	300
Merapi Wet Series[1]						
379-17	Basaltic-Andesite	2.23	19.7	1200	500	0
387-21	Basaltic-Andesite	2.23	19.3	1200	500	60
376-11	Basaltic-Andesite	2.23	17.5	1200	500	90
386-19	Basaltic-Andesite	2.23	19.3	1200	500	300
Vesuvius Wet Series[2]						
443-V5	Shoshonite	2.02	17.1	1200	500	0
442-V3	Shoshonite	2.02	17.9	1200	500	60
441-V1	Shoshonite	2.02	21.9	1200	500	90
445-V7	Shoshonite	2.02	21.7	1200	500	300

[1] Deegan et al. (2010)
[2] Jolis et al. (2013)
[3] Carbonate (wt. %) = Assimilant weight (mg) /(Assimilant weight (mg) + Glass weight (mg))

Table 2_revised
Click here to download Table: Blythe et al_Table 2_REVISED_UPLOAD.doc

Table 2. *Chemical compositions of starting materials.*

Oxide (wt. %)	Average composition of basaltic-andesite glass (anhydrous)[1]	1σ (10)[1†]	Average composition of basaltic-andesite glass (hydrated)[1]	1σ (9)[1†]	Average composition of shoshonite glass (hydrated)[2]	1σ (9)[2†]	Merapi limestone[1]	Vesuvius limestone[2]
SiO_2	54.11	0.60	51.83	0.43	49.85	0.21	0.28	0.02
TiO_2	0.85	0.09	0.89	0.05	1.03	0.08	0.01	-
Al_2O_3	18.98	0.17	18.08	0.24	15.95	0.67	0.13	-
FeO*	7.89	0.56	8.17	0.16	7.98	0.25	0.01	0.01
MnO	0.24	0.03	0.20	0.03	0.14	0.02	-	0.01
MgO	2.98	0.13	2.97	0.08	6.03	0.33	0.40	0.79
CaO	8.89	0.17	9.19	0.16	9.98	0.29	56.72	54.99
Na_2O	3.56	0.13	3.48	0.09	2.35	0.07	0.12	-
K_2O	2.05	0.10	2.05	0.03	4.01	0.19	-	-
P_2O_5	0.29	0.04	0.34	0.04	0.70	0.09	0.03	0.02
Total	99.85		97.20		98.02		57.70	55.84
H_2O	-		2.23		2.00		0.15	-
CO_2	-		-		-		44.93	44.11

[1]Deegan et al. (2010).
[2]Jolis et al. (2013).
[*] FeO reported as total Fe.
[†]1σ standard deviation; the number in parentheses represents the number of analyses for each sample.